AGU PUBLICATIONS

JGR

Journal of Geophysical Research: Space Physics

RESEARCH ARTICLE

10.1002/2013JA019513

Key Points:
- We preserve the historic Siple VLF transmitter data set
- Reception statistics from a 9 month period in 1986 favor quiet conditions
- We analyze the nonlinear growth and growth rate characteristics and trends

Correspondence to:
J. D. Li,
jdli@stanford.edu

Citation:
Li, J. D., M. Spasojevic, V. Harid, M. B. Cohen, M. Gołkowski, and U. Inan (2014), Analysis of magnetospheric ELF/VLF wave amplification from the Siple Transmitter experiment, *J. Geophys. Res. Space Physics*, *119*, 1837–1850, doi:10.1002/2013JA019513.

Received 3 OCT 2013
Accepted 24 FEB 2014
Accepted article online 27 FEB 2014
Published online 20 MAR 2014

Analysis of magnetospheric ELF/VLF wave amplification from the Siple Transmitter experiment

J. D. Li[1], M. Spasojevic[1], V. Harid[1], M. B. Cohen[2], M. Gołkowski[3], and U. Inan[1,4]

[1]Department of Electrical Engineering, Stanford University, Stanford, California, USA, [2]School of Electrical and Computer Engineering, Georgia Institute of Technology, Atlanta, Georgia, USA, [3]Department of Electrical Engineering, University of Colorado Denver, Denver, Colorado, USA, [4]Department of Electrical Engineering, Koc University, Istanbul, Turkey

Abstract Controlled experiments with dedicated ground-based ELF/VLF (0.3–30 kHz) transmitters are invaluable in investigating nonlinear whistler mode wave-particle interactions in the Earth's magnetosphere. The most productive such experiment operated between 1973 and 1988 near $L = 4$ at Siple Station, Antarctica. A major effort has been undertaken to digitize and preserve a significant portion of the historical data set from the original magnetic tapes, and we describe here the data set and the processing techniques used to remove artifacts introduced during recording and playback. We analyze a commonly transmitted diagnostic format from 1986 and present statistics on the occurrence and properties of amplified ELF/VLF waves received by a ground-based receiver at the geomagnetic conjugate location to Siple at Lake Mistissini, Quebec. For the interval examined, only 11% of Siple transmissions are successfully received in the conjugate hemisphere with quiet geomagnetic conditions being significantly more conducive to successful reception. The total growth for the events examined is estimated to be 5–40 dB, and nonlinear growth rates are in the range of 20–350 dB/s. The observations show that as the nonlinear growth rate increases, the duration of nonlinear growth decreases. Significant linear correlation is found between the noise floor and the saturation level, with higher noise floors resulting from increases in natural magnetospheric emissions. Finally, we find a lack of correlation between the nonlinear growth rate and the noise, threshold, and saturation levels.

1. Introduction

Discoveries in the 1950s and 1960s that man-made terrestrial radio signals in the extremely low frequency (ELF, 0.3–3 kHz) and the very low frequency (VLF, 3–30 kHz) bands trigger the generation of free-running emissions in the magnetospheric plasma led to interest in controlled experiments with dedicated transmission facilities [*Helliwell et al.*, 1964]. The most ambitious and prolific endeavor to date is the Siple Station experiment. During its operation from 1973 to 1988, the Siple Station experiment provided numerous observations of magnetospheric wave-particle and wave-wave interactions [*Helliwell*, 1970, 1979, 1988a; *Golkowski*, 2009], and it remains the preeminent source for validating computer simulations of whistler mode wave-particle interactions [*Gibby et al.*, 2008; *Hikishima and Omura*, 2012; *Nunn and Omura*, 2012].

Prior to the establishment of Siple Station, researchers observed VLF signals from Navy transmitters (20–30 kHz) arriving in the conjugate hemisphere with time delays consistent with magnetospheric propagation and accompanied by triggered emissions [*Helliwell et al.*, 1964]. When these transmitters broadcasted in Morse code, differences were observed in triggering behavior and signal growth between dots and dashes. This phenomenon was termed the dot-dash anomaly and indicated that triggering of VLF emissions relates directly to the duration of the injected signal [*Helliwell et al.*, 1964]. A dedicated and more flexible transmitter was needed to obtain better experimental data. Generating waves in the ELF/VLF bands, however, is a significant engineering challenge. The free space wavelength, on the order of hundreds of kilometers, renders a vertical antenna of comparable dimensions impractical. Horizontal antenna designs are inefficient because the Earth acts as a good conductor and produces near-field image currents [*Watt*, 1967]. It was observed that the ice sheet in Antarctica provides 2–3 km of dielectric isolation from the conducting ground and could be used to reduce near-field image currents. Early experiments at Byrd Station ($L = 7.25$) by the University of Washington failed to produce detectable echoes in the conjugate region as a result of the high latitude of the station and low antenna efficiency[*Helliwell and Katsufrakis*, 1974]. Recordings of abundant natural VLF activity near $L = 4$ at Eights Station suggested that a transmitter site at a lower latitude would be productive [*Helliwell et al.*, 1973] and led the way to the establishment of Siple Station.

Siple Station was established at 75.93°S, 84.25°W geographic, corresponding to an invariant latitude of 60.4°S, at $L = 4.2$ and with UT − MLT = +5. The magnetic conjugate point of the station was easily accessible, and a conjugate receiving station was deployed near Roberval, Quebec, Canada (48.52°N, 72.23°W) and then moved to Lake Mistissini (50.42°N, 73.87°W) in 1985 to reduce the increasing amount of local receiver noise due to industrial activity around Roberval [*Helliwell and Katsufrakis*, 1974; *Paschal*, 1988]. Construction of the station began in the austral summer of 1969/1970, and the station was named in honor of Paul Siple, an Antarctic pioneer and scientist. The original 21.2 km long dipole antenna was driven by an 80 kW transmitter until it was eventually upgraded in the austral summer of 1978/1979 to a 150 kW transmitter [*Carpenter and Bao*, 1983; *Golkowski*, 2009]. The antenna itself was extended in the austral summer of 1982/1983 to 42 km, with a second perpendicular dipole of the same length installed over two austral summers from 1984 to 1986 [*Gibby*, 2008] in order to efficiently couple into the whistler mode. By 1986, the Siple Station transmitter could radiate over 1 kW of ELF/VLF power, with antennas driven by a 150 kW source [*Raghuram et al.*, 1974; *Carpenter and Bao*, 1983]. This level of ELF/VLF radiated power available solely for scientific research remains unmatched to date. A more recent wave injection experiment using the High Frequency Active Auroral Research Program (HAARP) ionospheric heating facility to perform magnetospheric wave injection via ionospheric conductivity modulation yielded only 10–100 W of radiated ELF/VLF power during the most favorable geomagnetic conditions [*Platino et al.*, 2006; *Golkowski et al.*, 2008, 2010, 2011; *Cohen et al.*, 2010a; *Cohen and Golkowski*, 2013; *Jin et al.*, 2011].

The earliest Siple Station studies addressed the dot-dash anomaly and identified a minimum time duration for amplification. Using observations at the conjugate point in Roberval, Quebec, *Helliwell and Katsufrakis* [1974] found that the amplitude of tones of duration longer than 350 to 400 ms would reach some saturation level and no longer increase [*Helliwell and Katsufrakis*, 1974; *Helliwell*, 1983]. The signals underwent exponential growth on the order of 100 dB/s with total growth (measured as the difference between the saturation level and the identifiable initial level of the conjugate signal) on the order of 30 dB. This type of exponential temporal growth observed at a fixed location cannot be described by linear theory and remains an area of active research today [*Omura et al.*, 1991; *Gibby et al.*, 2008; *Omura and Nunn*, 2011; *Nunn and Omura*, 2012; *Hikishima and Omura*, 2012].

Subsequent studies built upon the increasing collection of formats transmitted from Siple Station and received at the conjugate stations. Due to the nature of the experiment's logistics and the contemporary data storage technology, observations were primarily investigated using a case study approach. Some basic statistics on the frequency of reception/nonreception with respect to magnetic conditions, on the tendency to see signals during quieting intervals, on seasonal and diurnal trends, and on path endpoint latitudes were compiled in the initial years of the experiment [*Carpenter and Miller*, 1976; *Carpenter and Bao*, 1983]. The most extensive statistical study to characterize the amplitude and temporal amplification of signals from Siple Station involved examination of a continuous 9 h period from January 1988 [*Carpenter et al.*, 1997; *Sonwalkar et al.*, 1997]. *Carpenter et al.* [1997] and *Sonwalkar et al.* [1997] analyzed the transmission of 109 cases, of which 52 cases were received. The minute-long format included a variety of transmitted elements, with particular attention paid to the receptions of 2 s long constant power pulses at 2400 Hz and 2 s long pulses in which the power was ramped up at 10 dB/s for the first second and held at constant power for the later second (the same type of pulses analyzed in the present paper). They found that the temporal growth rate ranged from ~20 dB/s to ~80 dB/s, amplified from initial amplitudes between 0 and 25 dB to reach saturation levels between 10 and 40 dB, relative to the noise level. They also found that there was no correlation between initial received signal power, saturation power level, and nonlinear signal growth rate, with the exception of a possible trend between the initial and the saturation levels which was explained as an artifact due to changes in ionospheric absorption from noon to postdusk. *Carpenter et al.* [1997] analyzed the same transmissions for reception of 200 ms pulses at 1900, 2150, and 2400 Hz. Their primary result was providing evidence for a spatial amplification process that accompanied the well-known exponential temporal growth to saturation. However, although *Carpenter et al.* [1997] and *Sonwalkar et al.* [1997] addressed a comparable number of cases, their implications are limited by the 9 h period of observation.

As a whole, limited quantitative statistical justification has been given for many other observations and conclusions that have appeared in the literature. Statistical analysis of signal characteristics over longer time periods was not previously possible due to physical limitations on examining the data, which required processing information stored on magnetic tapes to make 35 mm spectrogram records [*Gibby*, 2008], and the computational requirements for analyzing the data, with at best real-time processing speed toward

the last few year of operation at Siple [*Paschal*, 1988]. Most of the known quantitative numbers reported have been compiled from observations of single occurrences. For example, *Paschal* [1988] provides a survey of observed phenomena, including many unique individual cases. This may have also contributed to some success bias in reception statistics in that only strong and exceptional cases were selected for detailed case study.

The lack of rigorous long-term statistics resulted in many key parameters being coarsely estimated from early case studies which may not have been fully representative. For example, total temporal growth estimates of 30 dB and growth rates of 30–200 dB/s were repeatedly reported in the literature [*Helliwell et al.*, 1980; *Helliwell*, 1988a, 1988b]. Today, it is difficult to track down which specific observations yielded these early estimates. Precise estimation of these parameters can be a powerful tool in guiding current computer simulation efforts.

In recent years, a major effort to preserve and restore data from the Siple Station experiment has been undertaken [*Gibby et al.*, 2008]. We describe here our efforts in digitizing the historic data sets from Siple, Roberval, and Lake Mistissini and present statistics on signal growth rates and total growth using a specific transmitter format and data from April to December 1986.

2. Data Digitization and Timing Correction

During the Siple Transmitter experiment, the data were recorded by ELF/VLF receivers at Siple, Roberval, and Lake Mistissini using high-quality professional Ampex recorders and stored on magnetic tape reels [*Paschal*, 1988]. Periodically, the magnetic tape reels were shipped to Stanford University for analysis and storage. Because of the use of analog tapes, it is fairly common for errors to show up postdigitization. Frequency drift and timing error artifacts occur when the tape flutters or skips during reading. Fortunately, a number of identifying characteristics were consistently employed and were well documented for later scientific analysis of the transmitted data. In the continuous recordings made at Lake Mistissini in 1986, the data stored on the magnetic tape reels included two different features to provide timing data for reference and a calibration tone for the recording machine. Every 5 min, an 8 s long timing announcement using the Inter-Range Instrumentation Group B (IRIG-B) standard time code was injected. The timing announcement interrupted and overwrote any other data received at that time. All other data included a constant 10 kHz pilot tone modulated with second markers every second and encoded with a Morse code sequence at the start of every minute that identified the recording station, the number of days into the year, and the hour and minute. Every 5 min, following the timing announcement, a 1 s calibration tone at 5 kHz was provided. The data also capture the broadcasts of other transmitters of known frequency and timing, namely the United States Omega transmitters and the Russian Alpha transmitters [*Paschal*, 1988].

2.1. Data Digitization

In recent years, a large portion of the analog magnetic tapes from the Siple Station experiment has been digitized. The digitization efforts have focused on the ELF/VLF recordings made locally at Siple and in the conjugate region at Roberval and Lake Mistissini using magnetic field sensors similar to those as described in *Harriman et al.* [2010] and *Cohen et al.* [2010b]. Some selected intervals of data from the International Satellites for Ionospheric Studies (ISIS), which provided low altitude in situ observations of Siple transmissions, have also been digitized. The magnetic reel tapes were played back on an Ampex-440C Recorder/Reproducer and digitized by passing the signal through an antialiasing Rockland Systems Corporation Model 452 Hi/Lo Pass Filter to a National Instruments 6013 data acquisition card. The system passes through data with signals ranging up to 25 kHz and provides a signal-to-noise ratio of around 50 dB. Figure 1 illustrates the number of hours of data digitized as a function of month and year for each of the four receivers. Altogether, 6972 h of data have been digitized for a total of 2.51 TB of data. Given the difficulty in comprehensive digitization of the data after the experiment, it is difficult to estimate with certainty the total amount of data. Estimates based on the total amount of data still in storage puts the percentage of digitized data at around 20%.

2.2. Timing Correction

Data digitized from magnetic tapes often exhibit artifacts of frequency drifts and timing errors, which can be largely corrected by examining the deviations in the phase of the 10 kHz pilot tone as first proposed by *Paschal and Helliwell* [1984]. As the tape speed fluctuates, at either recording or playback, the observed pilot

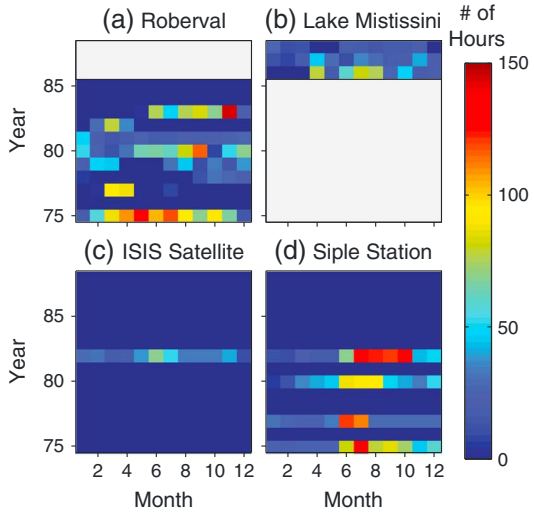

Figure 1. Number of hours of digitized data as a function of month and year during the Siple Station experiment. Each panel corresponds to one of four receivers, located at (a) Roberval, Quebec, (b) Lake Mistissini, Quebec, (c) ISIS satellite, and (d) Siple Station, Antarctica. The Lake Mistissini receiver replaced the Roberval receiver in 1986. The whitened-out portion of the plots indicate the years when the receiver was not in operation.

tone frequency drifts from 10 kHz resulting in a measurable advance or delay in the phase of the signal. To correct the frequency drift, we first apply a 175 Hz narrowband filter around the pilot tone frequency to obtain a set of sampled points from the pilot tone, y_f. The samples are complex, allowing for the use of phasor notation to represent the points by a magnitude and phase.

As the tape speed fluctuates, the phase of the pilot tone also changes. By taking a cumulative sum over a given time step consisting of n samples, we obtain the cumulative phase drift and magnitude, y_{total} as follows:

$$y_{\text{total}} = \sum_{k=1}^{n} y_f[k] \tag{1}$$

Here n is set to 14 samples, or 0.56 ms of data, to handle any rapid frequency changes.

In phasor notation, we can represent y_{total} as an arc of some circle in the complex plane that geometrically describes the cumulative phase drift and magnitude of the signal. We can find the length of the chord, l, that subtends the arc and estimate the radius of the implicit circle, r_c. Then, the total change in phase, θ_c, the difference in phase over one time step, can be found from the geometry of the circle as

$$\theta_c = 2 * \sin^{-1}\left(\frac{l}{2 * r_c}\right) \tag{2}$$

The frequency correction, f_{corr}, is by definition the change in phase, θ_c, over the change in time and can be calculated as

$$f_{\text{corr}} = \frac{\theta_c}{2\pi n} \tag{3}$$

By taking the cumulative sum of f_{corr} and dividing by the sampling frequency, f_s, we can interpolate and find the change in timing from the original signal, t_{interp}, as

$$t_{\text{interp}} = \frac{1}{f_s}\sum_{k=1}^{n} f_{\text{corr}} \tag{4}$$

By scaling the timing drift, t_{interp}, with the ideal pilot tone frequency of 10 kHz, we obtain the timing difference that would result in the observed signal frequency offset. Then, we simply add this difference back to the measured signal time, t_{signal} in order to recover the timing that would correspond with a 10 kHz tone and thus recover the original timing as

$$t_{\text{corr}} = t_{\text{signal}} + \frac{t_{\text{interp}}}{f_{\text{pilot}}} \tag{5}$$

Although the timing correction is calculated only for the pilot tone, the drift in frequency and timing is assumed to be constant across frequencies, and so the correction applies to the entire signal. An example of this applied correction is illustrated in Figure 2, which shows the pilot tone before and after correction. In Figure 2a, noticeable fluctuations in the pilot tone can be seen, with spikes that deviate up to 200 Hz, and similar errors in the Omega transmitter tone at 10.2 kHz. In Figure 2b, the data have been corrected, with a majority of the pilot tone present in its 10 kHz band and similarly for the Omega tone. We also see a correction in the timing with a shift of some 5 s in this example that occurred as a result of correcting 60 min of the

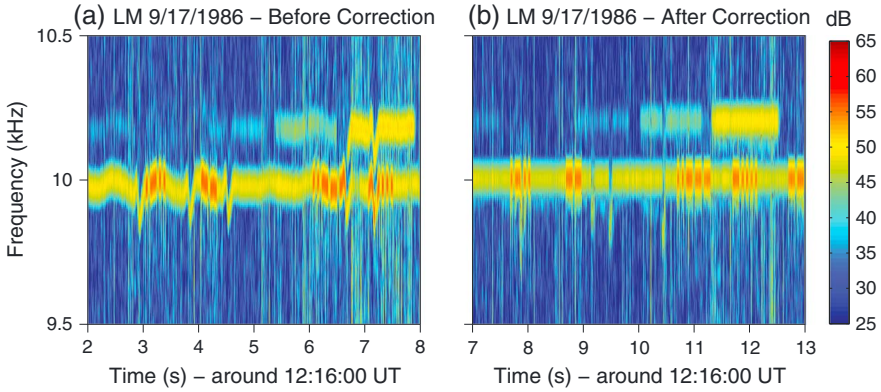

Figure 2. Timing Correction Example. A section of data from the Lake Mistissini receiver from 17 September 1986 illustrating the results of the timing correction algorithm. (a) The data prior to timing correction and (b) the data after timing correction.

data file. While this example exhibits more serious timing errors (in this case some of the spikes in the 10 kHz pilot tone were completely outside of the 175 Hz narrowband filter and were not completely corrected), it is common to see the occurrence of some amount of error, and a majority of the digitized data require timing correction. The timing correction procedure was developed specifically for data from 1986 and may require some adaptation for data from other years.

3. Statistical Observations From 1986

While prior studies of data from Siple Station transmissions have largely been concerned with examining individual cases with exceptional signal strength or triggered emissions, we present a more focused study of a single transmission format over the course of 9 months from April to December of 1986. The statistics on transmission reception provide some insight into the conditions governing successful conjugate wave transmissions, and an examination of signal amplitudes and growth rates provides quantification of key parameters in the magnetospheric wave-particle interaction.

3.1. The MDIAG Format

Although many different formats were transmitted from Siple Station during its years of operation, we focus on the minidiagnostic or MDIAG format from 1986. It is illustrated in Figure 3a and begins with a 2 s tone at the central tuning frequency, or f_{set}, with an amplitude ramp starting at −10 dB that rises at 10 dB/s for the first second until reaching and holding constant at 0 dB for the remaining second. The 2 s tone is followed by a descending staircase of five 200 ms long tones spaced 250 Hz apart from f_{set}+500 to f_{set} − 500, two descending frequency ramps (the first at 0 dB and the second at −6 dB) over the same frequency range for 1 s each, and a 7 s long pair of constant frequency tones (called a doublet) at f_{set} + 480 and at f_{set} + 510 at 0 dB. The central tuning frequency was selected for each transmission by the operator based on his evaluation of natural conditions. In this study, we focus on the 2 s tone at the start of the format. At reception, the linear growth phase where the signal retains its built-in 10 dB/s amplitude ramp at the beginning of the tone can be differentiated from the nonlinear growth phase where the signal amplitude increases at a significantly higher rate, allowing for some insight into the behavior of transmitted signals undergoing magnetospheric amplification. The built-in amplitude ramp allows for calculation of the threshold level, which marks the transition to the phase of nonlinear signal growth. At saturation, the signal is commonly accompanied by the presence of triggered emissions, which are narrowband emissions that begin near the original signal and then sweep through a wide range of frequencies [*Helliwell*, 1979; *Omura et al.*, 1991].

Figure 3 shows an example of the MDIAG format at transmission and reception using a spectrogram, which displays the time-frequency plot with amplitude strength marked by the color bar, and a visual illustration of the automated detection process. Figure 3a is a spectrogram view of the signal format, as described, that would be transmitted from Siple Station. It is time aligned with Figure 3b, which shows an actual received signal at the Lake Mistissini receiver, including the path delay. The signal was received cleanly and all components of the format were clearly preserved although some portions may be less distinct due to the reception of overlapping triggered emissions.

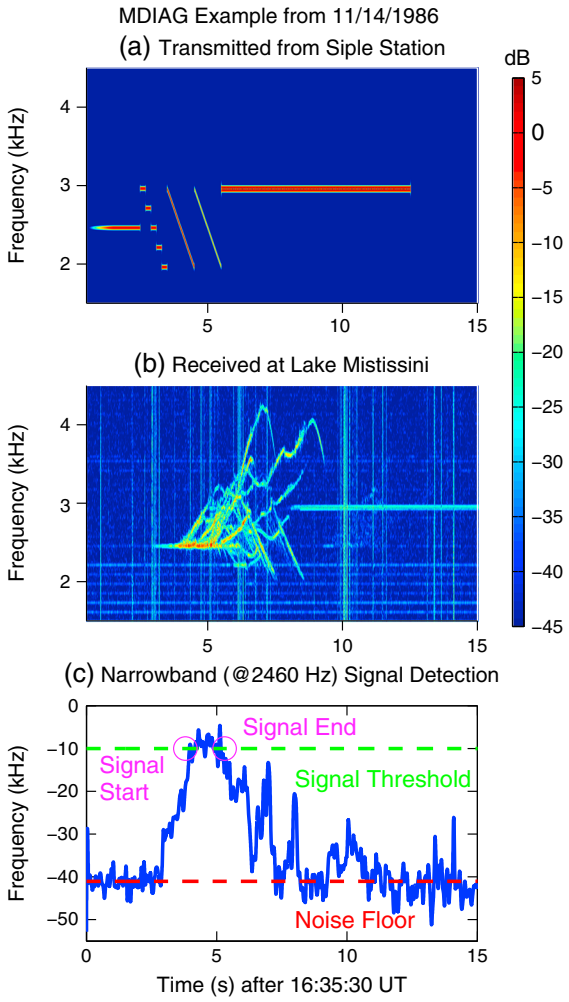

Figure 3. MDIAG Example. (a) The transmission format from Siple Station, (b) a received signal with triggered emissions as recorded at Lake Mistissini, (c) the main tone amplitude at the f_{set} frequency of 2460 Hz illustrating the detection of the signal using a signal threshold technique.

3.2. Automated MDIAG Detection

With over 4000 transmissions of MDIAG in 1986, we employ an automated detection algorithm in order to build a data set of received signals for analysis. The method is illustrated in part by Figure 3c. We process the 1986 scanned transmission logs using an optical character recognition software in order to extract the time and the f_{set} for each MDIAG transmission. After searching the data for each transmission, we filter the data using a narrowband (100 Hz) filter around the f_{set} frequency (which is 2460 Hz in Figure 3) and examine the signal amplitude for the distinctive occurrence of the 2 s tone. Using Otsu's method, which calculates the threshold value that maximizes interclass variance to separate data into a foreground and a background, we set a threshold, shown by Figure 3 (dotted green line), for separating the signal from the noise floor [*Otsu*, 1979]. By checking if the duration of the signal passing the threshold exceeds 0.35 s, we filtered out cases dominated by higher-intensity radio atmospheric signals (sferics), which are short in duration and retained cases with the successful reception of an MDIAG transmission. Visual verification of the detected cases afterward shows that this process performs fairly well, detecting ~85% of the received signals. While this method may require some refinement, many of the false negatives involve substantially weaker signals, cases where only a portion of the format (for instance the lower two tones in the staircase) were received, or cases where a large number of sferics obscure the signal.

3.3. Reception Statistics

Table 1 gives reception statistics for the data set. The reception statistics differ from previous work in that we only consider the MDIAG transmission format, as opposed to counting all signals that were observed in some duration [*Carpenter and Bao*, 1983; *Carpenter and Miller*, 1976; *Golkowski et al.*, 2008]. As the data were not available for all 4000 MDIAG transmissions (some data tapes have not been located), our study consists of the 942 MDIAG transmissions that were available, of which 106 cases, 11.3%, were received at Lake Mistissini, the conjugate point. In the case of daytime (sunlight at 100 km) operations at Siple Station, 55 of 599 (9.2%) transmissions were received; while in the nighttime (darkness at 100 km) at Siple Station, 51 of 343 (14.9%) transmissions were received. We consider the daytime and nighttime conditions only at Siple, as only 16 cases were transmitted, with only one case received, during the nighttime at Lake Mistissini and the other 926 cases occurred during the daytime at Lake Mistissini. These reception statistics are lower than earlier results for reception of all one-hop echoes

Table 1. Table of MDIAG Reception Statistics in 1986, Broken Down by Day/Night Conditions at the Siple Station Transmitter

	Day Time	Night Time	All Cases
Number Transmitted	599	343	942
Number Received	55	51	106
Percentage Received	9.2	14.9	11.3

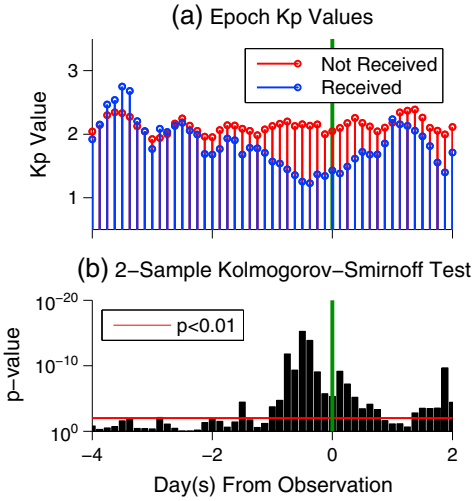

Figure 4. (a) Superposed epoch analysis of the average *Kp* index over a 6 day period for MDIAG transmissions detected in the conjugate hemisphere in blue and those transmitted but not detected in red. (b) *P* values for a two-sample Kolmogorov-Smirnoff statistical significance test are plotted for each 3 h epoch interval. Note, the *y* axis is inverted such that smaller *p* values appear as taller bars to visually indicate significance.

[*Carpenter and Bao*, 1983] as the detection criteria here is specific to the MDIAG format and requires that the 2 s tone at the beginning of the MDIAG be measurable rather than merely detectable.

Next, we examine the geomagnetic conditions surrounding the time of transmission, noting that 1986 was a year of overall low geomagnetic activity near the solar cycle minimum. We perform a superposed epoch analysis using the *Kp* index examining conditions from 4 days before to 2 days after the time of transmission. Figure 4 shows the average *Kp* in 3 h increments in blue for all the cases when the MDIAG format was successfully received in the Northern Hemisphere and in red for times when the format was transmitted but not detected. To test the statistical significance of the differences in *Kp* values between received and not received cases, we apply a Kolmogorov-Smirnov test to evaluate if the sampled values are drawn from different underlying distributions, and note that the period of quieting leading up to the hour of transmission is statistically different for received cases, with $p < 0.01$. A similar analysis performed with magnetospherically injected signals from the HAARP facility showed a similar trend [*Golkowski et al.*, 2011].

3.4. Amplitude and Growth Trends

Next, we examine characteristics of the signal amplitudes and growth rates for the set of 106 MDIAG receptions. In order to meaningfully consider signal amplitude parameters between transmissions from different data files, we need to consider the signal-to-noise ratio at the receiver, which strongly depends on both the fixed electronic noise of the receiver and the highly variable natural noise from chorus, hiss, and lightning. The variable noise floor complicates our analysis as portions of the MDIAG reception may be below the noise floor and thus inaccessible. Lightning-generated impulses tend to dominate the injected noise characteristics [*Chrissan and Fraser-Smith*, 1996] but can be successfully removed with preprocessing. We can also eliminate the effects of variability in measurements from the different Ampex machines used to record data at each site by normalizing values to the constant calibration tone injected into the receiver.

We focus on the 2 s tone at the beginning of the MDIAG format, as mentioned in section 3.1, to obtain measurements in the following manner. First, we take 4 s of broadband data centered on the estimated time of arrival of the tone and apply a preprocessing technique to remove sferics developed within our research group. Here, we use an adaptive threshold to detect impulsive noise and, assuming that the noise changes quickly as compared with the signal of interest, then model the impulsive noise using a multivariate autoregressive model to remove sferics. Then, we multiply the broadband signal by a complex exponential in order to shift it down to baseband from the f_{set} carrier frequency specified in the transmission logs. Using a low-pass filter with a 100 Hz bandwidth, we extract the narrowband signal. After smoothing with a 10-point median filter to further reduce impulsive noise, we normalize the signal using the closest preceding reference calibration tone. The narrowband signal amplitudes for all 106 cases provide measurements of the saturation power level and the nonlinear growth rate as illustrated in Figure 5a. Here, the noise floor (Figure 5, dashed red line) dominates until the high nonlinear growth rate (Figure 5, dashed orange line), 159.5 dB/s in this case, causes the signal to rise out of the noise floor. Growth then stops at saturation (Figure 5, dashed green line). However, for a subset of 14 cases, identified here as Subset 1, additional parameters of the signal can be quantified as shown in Figure 5b. The distinguishing feature of Subset 1 is that the initial signal level (Figure 5, dashed black line) is distinct from the noise floor. Next, the built-in 10 dB/s amplitude ramp (Figure 5, dashed yellow line) can be seen. At some amplitude level, indicated as the nonlinear threshold (Figure 5, dashed cyan line), the growth rate drastically increases. The signal grows at this higher nonlinear growth rate until it reaches saturation as before.

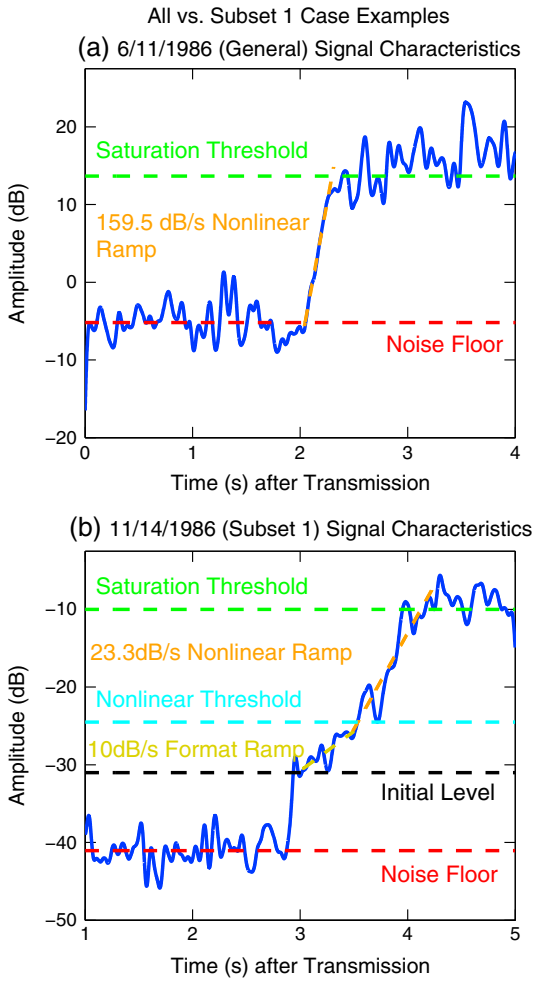

Figure 5. (a) General and (b) Subset 1 MDIAG cases. General cases describe the cases where the signal rises up from the noise floor (dashed red line), undergoes nonlinear amplification (dashed orange line), and then saturates (dashed green line). Subset 1 cases describe cases where the signal is received clearly distinct from the noise floor (dashed red line) at some initial power level (dashed black line), undergoes a phase of linear amplification that can be identified by the presence of the injected 10 dB/s amplitude ramp (dashed yellow line), reaches some growth threshold (dashed cyan line), experiences nonlinear amplification (dashed orange line), and then saturates (dashed green line).

For an MDIAG signal to be received at Lake Mistissini, the transmitted whistler mode VLF wave typically experiences some type of cyclotron resonance growth as a result of interaction with energetic electrons in the near-equatorial magnetosphere. The growth resulting from this interaction can be divided into two phases: (1) linear or spatial growth wherein all portions of the signal are amplified to the same degree and (2) nonlinear or temporal growth wherein later portions of the signal are amplified more than earlier portions. The MDIAG format was designed in order to excite wave amplification and evaluate the power threshold needed to trigger nonlinear amplification [*Helliwell et al.*, 1980]. For this reason, the format includes a 10 dB/s amplitude ramp at the start of the transmission. For the Subset 1 cases, the signal growth from the initial level to the saturation level goes through two distinct phases. Figure 5b clearly shows that the first amplitude ramp is 10 dB/s (equivalent to the power increase at the transmitter). This observed 10 dB/s amplitude ramp is indicative of the phase of linear signal growth. The originally transmitted 10 dB/s amplitude ramp is preserved and all portions of the received signal are amplified by the same amount according to expectations from linear theory. The amount of linear growth itself is not measurable by a ground-based VLF receiver precisely because all portions of the signal are amplified identically. At the nonlinear threshold level, the amplitude slope suddenly switches to exceed the original 10 dB/s slope. This portion is indicative of temporal growth as later portions of the signal are amplified more than earlier portions. In the majority of received cases, only the later, temporal or nonlinear growth portion of the signal is detectable, and the nonlinear growth rate is determined by measuring the slope of the signal power as it rises from the noise floor to the saturation level.

Past observational studies [e.g., *Helliwell et al.*, 1980; *Helliwell*, 1988a; *Sonwalkar et al.*, 1997] refer to the two phases of observed signal growth as the spatial and temporal (or exponential) growth phases. However, more recent theoretical works [e.g., *Omura et al.*, 2008; *Gibby et al.*, 2008] have shown that the two growth phases can be described by linear and nonlinear theory, respectively. In order to focus on physical processes rather than observed phenomena, we will henceforth refer to the growth phases as linear and nonlinear.

First, we consider the general set of cases, for which only the nonlinear growth portion is visible and analyze the saturation level, the nonlinear growth rate, the noise floor, and the f_{set} tuning frequency. Figure 6a shows the lack of statistically significant correlation between the nonlinear growth rate and the saturation power level, that is, a higher nonlinear growth rate does not necessarily result in higher signal amplitude (consistent with the results from *Sonwalkar et al.* [1997]). We do, however, find a moderate ($\rho = 0.6$) but statistically significant ($p < 0.05$) correlation between the noise floor and the saturation power level as shown

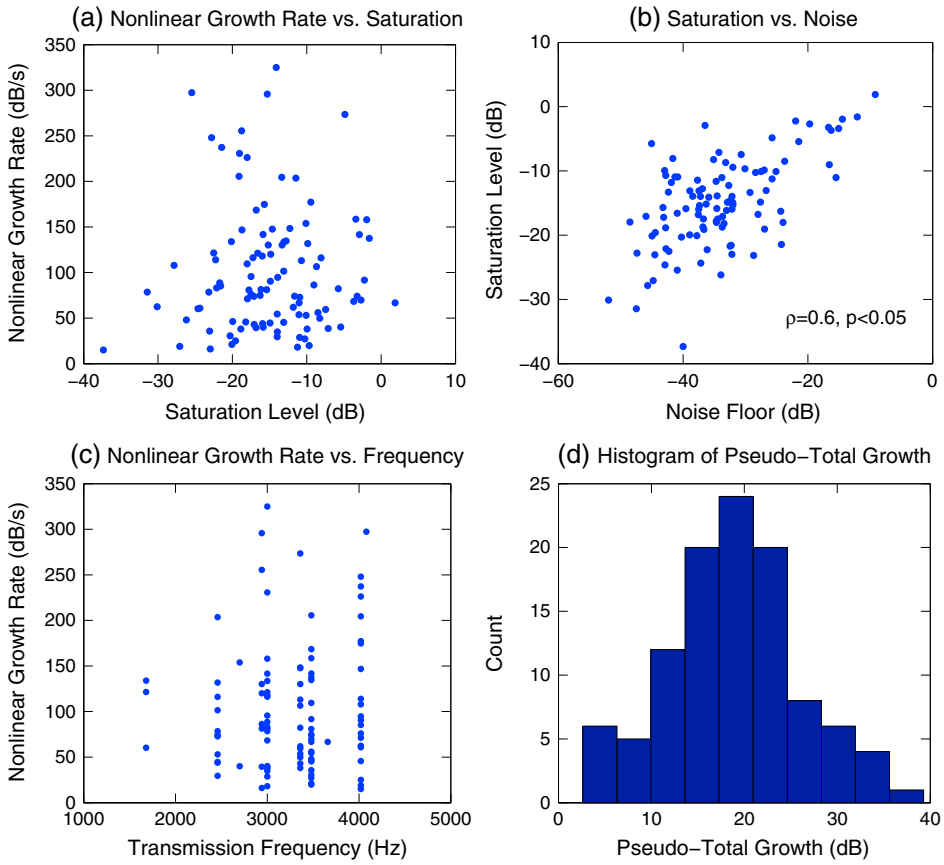

Figure 6. Comparison amongst saturation power level, the nonlinear growth rate, and the noise floor using the set of all general cases. Values of ρ are given only for statistically significant, $p < 0.05$, correlations. (a) The nonlinear growth rate compared against the saturation power level, (b) the saturation power level compared against the noise floor [$\rho = 0.60$ $p < 0.05$], (c) the nonlinear growth rate compared against the f_{set} tuning frequency, and (d) a histogram of pseudo-total growth.

in Figure 6b. The noise floor in the band of Siple transmission is highly variable, covering a range of about 40 dB. Since preprocessing of the data includes sferic removal, the remaining variability in the noise floor is largely due to occurrence of magnetospheric emissions including bands of hiss or chorus. As further discussed in section 4, this suggests that when conditions are favorable for the linear amplification of magnetospheric noise, Siple signals are also able to achieve higher total amplitude. However, the rate at which signals grow to saturation appears to be independent as the nonlinear growth rate is not correlated with either the saturation level (Figure 6a) or the noise level (not shown).

Figure 6c examines the nonlinear growth rate as a function of the f_{set} transmission frequency. There are relatively few columns as only a fixed number of discrete f_{set} frequencies were used for transmissions. Overall there is no correlation between nonlinear growth rate and f_{set}, and furthermore, for a given f_{set}, the nonlinear growth rate is relatively uniformly spread over a wide range of values (consistent with the results from *Carpenter et al.* [1997]). We note that all transmissions were below 0.5 of the equatorial gyrofrequency, which for the location of Siple corresponds to about 6 kHz.

To compare with earlier work by *Helliwell and Katsufrakis* [1974] and *Helliwell et al.* [1980], we also measure the total amplification from the noise floor, which is termed the total growth in past literature. We redefine that here as the pseudo-total growth as it does not include any signal growth that may have occurred below the noise floor. Figure 6d is a histogram of such pseudo-total growth, calculated as saturation level minus noise floor, for all of the cases and shows a spread of 5–40 dB and a maximum number of occurrences just under 20 dB. While these values are not significantly different from past work by *Helliwell and Katsufrakis* [1974] and *Helliwell et al.* [1980], the oft cited 30 dB value should likely be adjusted to ~20 dB. While this

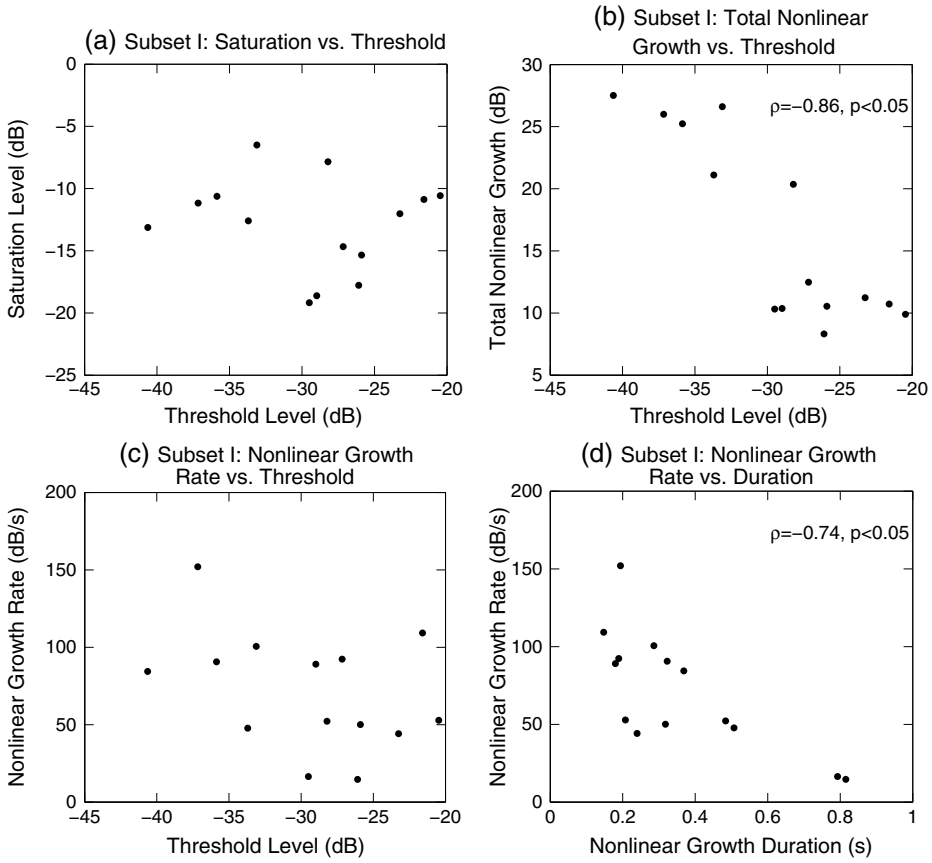

Figure 7. Comparison amongst threshold power level, saturation power level, total growth, and the nonlinear growth rate and duration using the set of cases where the initial and threshold power levels were clearly distinguishable from the noise floor. Values of ρ are given only for statistically significant, $p < 0.05$, correlations. We compare (a) the saturation power level, (b) the total growth, and (c) the nonlinear growth rate with the threshold power level, and (d) the nonlinear growth rate with the nonlinear growth duration.

new value only definitively applies to data from 1986, this update has more statistical justification than the original value and may tentatively be used in the general case.

Next, we examine the 14 Subset 1 cases, which occurred on four separate days and include measurements of the nonlinear threshold level, that is the amplitude at which the growth changes from linear to nonlinear. Figure 7a compares the saturation level with the threshold level. There is no statistically significant correlation, implying that the total nonlinear growth should decrease as the threshold level increases. This, in fact, can be seen in Figure 7b, which plots the total nonlinear growth against the threshold level and shows strong negative correlation ($\rho = -0.86$, $p < 0.05$). The total nonlinear growth is in the range of 5–30 dB.

Further, the nonlinear growth rate is also uncorrelated with both the threshold level (Figure 7c) and the saturation level (not shown, but consistent with Figure 6a). Finally, in Figure 7d we see the strong negative correlation ($\rho = -0.74$, $p < 0.05$) between the nonlinear growth rate and the nonlinear growth duration. Signals with higher nonlinear growth rates grow for a shorter time period while signals with lower growth rates grow for a longer time period.

4. Discussion

The statistical analysis of data from the Siple Station experiment enables observation-driven evaluation of physical models of resonant, nonlinear growth. The analysis presented here provides statistical verification of generalized observations from past work and provides insight to theoretical studies. Current prevailing theory holds that temporal growth and the generation of free-running emissions is the result of nonlinear

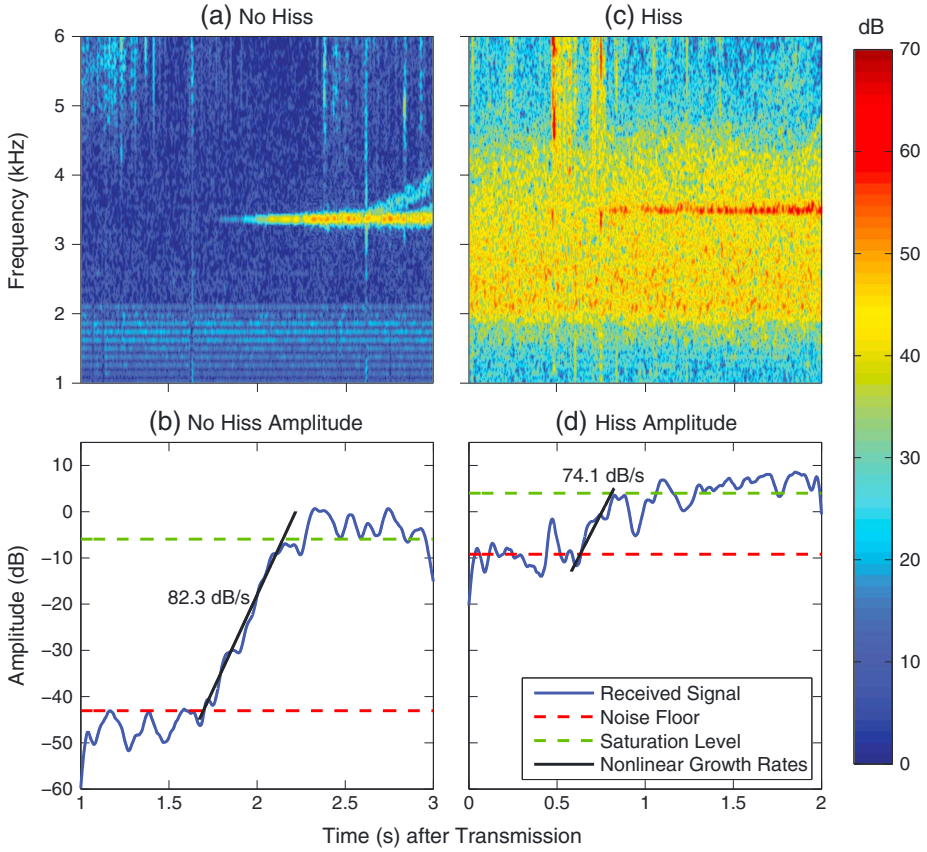

Figure 8. Comparison of two received transmissions with and without hiss. The spectrograms show (a) the lack of and (b) the presence of a hiss band. The corresponding narrowband analysis at the f_{set} transmitter frequency shows Figure 8a has lower noise and saturation levels for the no hiss transmission, and Figure 8b has higher noise and saturation levels for the transmission with hiss, even though the nonlinear growth rates are similar.

gyroresonant interactions between whistler mode waves and resonant particles [*Omura et al.*, 1991; *Hikishima and Omura*, 2012; *Nunn and Omura*, 2012]. As shown in Figure 5b, the injected signal grows first according to linear theory and then, after passing the power threshold, abruptly switches to a regime of nonlinear growth. This is generally attributed to nonlinear phase trapping of resonant electrons. As particles move away from the equator, there is a finite wave amplitude required for trapping. Recent work on the theory using numerical simulations, previously limited due to insufficient computing capability, has also demonstrated that the trapping mechanism results in a depletion of electron density in phase space known as a "phase space hole" which appears to be responsible for many of the nonlinear effects. The formation of this phase space structure, which takes a finite amount of time, along with the finite amplitude for trapping may be responsible for the finite transition time between linear and nonlinear growth [*Dowden et al.*, 1978; *Vomvoridis and Denavit*, 1979; *Omura et al.*, 2008; *Hikishima and Omura*, 2012].

The analysis of 2 s tones transmitted by Siple and received in the conjugate hemisphere allows us to statistically quantify the nonlinear growth rate, saturation level, and estimate the total signal growth. The transmission format includes a 10 dB/s amplitude ramp during the first second, which allows us, in a small subset of cases, to separate the linear growth phase from the nonlinear growth phase and determine the threshold amplitude at which that occurs. We find that the nonlinear growth rate varies between ~20 and 350 dB/s, but the nonlinear growth rate does not depend on (1) the transmission frequency (within a narrow range below 0.5 of the equatorial gyrofrequency), (2) the noise floor, (3) the threshold amplitude, or (4) the saturation level. The lack of correlation between these quantities suggests that once a signal reaches the threshold amplitude, it will proceed to undergo nonlinear growth, but our observations do not provide insight on what controls the value of the nonlinear growth rate.

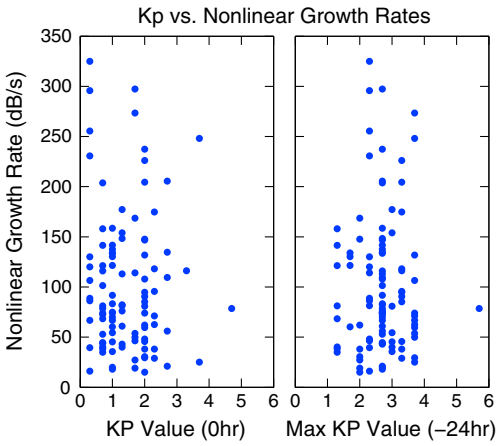

Figure 9. Two-panel figure correlating nonlinear growth rate in dB/s with the *Kp* index for all cases. (left) Comparison of the nonlinear growth rate with the *Kp* value at the time of transmission and reception, and (right) the same comparison with the maximum *Kp* value in the last 24 h.

Further, we find that as the nonlinear growth rate increases, the nonlinear growth time decreases. Also, as the threshold level increases, the total nonlinear growth decreases. Both of these observations suggest that the saturation level, though not constant, is bounded.

We also find that the saturation level is linearly correlated with the measured noise floor. Lightning generated sferics contribute significantly to the noise floor in this frequency range, and two data processing techniques were used to minimize the effects on sferics on the data (autoregressive sferic removal on the broadband data and median filtering of the extracted narrowband signal). Even after sferic removal, the noise floor during the observations varies over a range of ~50 dB, as seen in Figure 6b. In examining the individual case records, we find that events with significantly higher noise (above −15 dB) often occur in the presence of a band of magnetospheric emissions such as hiss and chorus. Figure 8 shows two example records with and without the presence of a band of hiss. The hiss band contributes to a 35 dB higher noise floor (Figure 8, red dashed line), and the saturation amplitude in the hiss case is 11 dB higher. The nonlinear growth rate for the two cases is similar (Figure 8, black line), but the duration of observed nonlinear growth is nearly twice as long for the transmission without a hiss band. These observations indicate the possibility that stronger magnetospheric activity correlates with higher saturation and noise levels, and this suggests that the saturation level is influenced by the linear growth rate. In contrast the lack of correlation between the nonlinear growth rate and saturation, threshold and noise level suggests that the nonlinear growth rate is somewhat independent of the linear growth rate.

To further investigate these ideas, we correlate the nonlinear growth rate and the saturation level with measures of the geomagnetic activity. Figure 9 plots the maximum value of the *Kp* index in the 24 h preceding the Siple transmission with (Figure 9a) the saturation level and (Figure 9b) the nonlinear growth rate but shows no correlation in either quantity. Comparisons with the *AE* and *SYM-H* index produce a similar lack of correlation. It is likely that the global nature of geomagnetic indices does not well represent condition in an isolated magnetospheric duct and that the presence of natural emissions remains the best indicator of local conditions for wave growth.

5. Conclusions

A major effort has been undertaken to restore and preserve data collected during the Siple Transmitter experiment. Nearly 7000 h of data have been digitized from magnetic tapes, and algorithms have been developed to eliminate frequency drifts and timing errors inherent in the data. The analysis presented here focuses on a frequently transmitted diagnostic format (MDIAG) that included a 2 s tone and allows for determination of the nonlinear growth rate, saturation level, and an estimate of the total growth, which is dubbed the pseudo-total growth as it cannot take into account growth from below the highly variable noise floor. In a subset of cases the phases of linear and nonlinear growth can be separated.

For the 1986 interval examined here, the reception rate of the MDIAG format is relatively low with only ~11% of MDIAG transmissions from Siple being clearly detectable in the conjugate hemisphere. Dark ionospheric conditions at the transmitter led to slightly higher (~15%) reception rates, likely due to decreased transionospheric absorption [e.g., *Graf et al.*, 2013]. We find that the average geomagnetic conditions, as described by the *Kp* index, for successful transmissions are characterized by a highly statistically significant period of quieting compared with the undetected transmissions. At the time of transmission, the *Kp* index is 0.84 units lower when the signal is received than when it is not. This matches with similar observations made by *Golkowski et al.* [2011] for the successful reception of two-hop signals using HAARP. *Golkowski et al.* [2011] interpreted the correlation of conjugate reception to geomagnetic quieting as stemming from

the conditions for optimum stability of ducted propagation paths. The results here are consistent with that interpretation.

The pseudo-total growth for the events examined here is in the range of 5–40 dB with a maximum number of occurrences at 20 dB, and the nonlinear growth rates are in the range of 20–350 dB/s. The observations show that as the nonlinear growth rate increases the duration of nonlinear growth decreases, and also that as the threshold amplitude (the amplitude at which growth changes from linear to nonlinear) increases the total nonlinear growth decreases. Both of these observations suggest that the saturation level is bounded. Further, the correlation between saturation level and increases in the noise floor due to natural magnetospheric emissions suggests that the absolute saturation level is controlled by the linear growth rate. The lack of correlation between the nonlinear growth rate and the noise, threshold and saturation levels suggest that the nonlinear growth rate is independently controlled and may not depend on the linear growth rate.

Acknowledgments

This work is supported by AFRL award FA9453-11-C-0011 to Stanford University and subcontract 27239350-50917-B to CU Denver. We thank Ryan Said, Timothy Bell, and Donald Carpenter for helpful discussions. We thank Dan Musetescu for his tremendous help digitizing the data and Blane Wilson for his work processing the 1986 transmission logs.

Robert Lysak thanks Vikas Sonwalkar and Andrew Gibby for their assistance in evaluating this paper.

References

Carpenter, D. L., and Z. T. Bao (1983), Occurrence properties of ducted whistler-mode signals from the new VLF transmitter at Siple Station, Antarctica, *J. Geophys. Res.*, *88*, 7051–7057, doi:10.1029/JA088iA09p07051.

Carpenter, D. L., and T. R. Miller (1976), Ducted magnetospheric propagation of signals from the Siple, Antarctica, VLF transmitter, *J. Geophys. Res.*, *81*, 2692–2700, doi:10.1029/JA081i016p02692.

Carpenter, D. L., V. S. Sonwalkar, R. A. Helliwell, M. Walt, U. S. Inan, M. Ikeda, and D. L. Caudle (1997), Probing properties of the magnetospheric hot plasma distribution by whistler mode wave injection at multiple frequencies: Evidence of spatial as well as temporal wave growth, *J. Geophys. Res.*, *102*, 14,355–14,362, doi:10.1029/96JA03046.

Chrissan, D. A., and A. C. Fraser-Smith (1996), Seasonal variations of globally measured ELF/VLF radio noise, *Radio Sci.*, *31*(5), 1141–1152, doi:10.1029/96RS01930.

Cohen, M. B., and M. Golkowski (2013), 100 days of ELF/VLF generation via HF heating with HAARP, *J. Geophys. Res. Space Physics*, *118*, 6597–6607, doi:10.1002/jgra.50558.

Cohen, M. B., U. S. Inan, M. Golkowski, and M. J. McCarrick (2010a), ELF/VLF wave generation via ionospheric HF heating: Experimental comparison of amplitude modulation, beam painting, and geometric modulation, *J. Geophys. Res.*, *115*, A02302, doi:10.1029/2009JA014410.

Cohen, M. B., U. S. Inan, and E. W. Paschal (2010b), Sensitive broadband ELF/VLF radio reception with the AWESOME instrument, *IEEE Trans. Geosci. Remote Sens.*, *48*, 3–17, doi:10.1109/TGRS.2009.2028334.

Dowden, R. L., A. D. McKay, L. E. S. Amon, H. C. Koons, and M. H. Dazey (1978), Linear and nonlinear amplification in the magnetosphere during a 6.6-kHz transmission, *J. Geophys. Res.*, *83*(A1), 169–181, doi:10.1029/JA083iA01p00169.

Gibby, A. R. (2008), Saturation effects in VLF triggered emissions, PhD dissertation, Stanford University, United States – California.

Gibby, A. R., U. S. Inan, and T. F. Bell (2008), Saturation effects in the VLF-triggered emission process, *J. Geophys. Res.*, *113*, A11215, doi:10.1029/2008JA013233.

Golkowski, M. (2009), Magnetospheric wave injection by modulated hf heating of the auroral electrojet, PhD dissertation, Stanford University, Stanford, Calif.

Golkowski, M., U. S. Inan, A. R. Gibby, and M. B. Cohen (2008), Magnetospheric amplification and emission triggering by ELF/VLF waves injected by the 3.6 MW HAARP ionospheric heater, *J. Geophys. Res.*, *113*, A10201, doi:10.1029/2008JA013157.

Golkowski, M., U. S. Inan, M. B. Cohen, and A. R. Gibby (2010), Amplitude and phase of nonlinear magnetospheric wave growth excited by the HAARP HF heater, *J. Geophys. Res.*, *115*, A00F04, doi:10.1029/2009JA014610.

Golkowski, M., M. B. Cohen, D. L. Carpenter, and U. S. Inan (2011), On the occurrence of ground observations of ELF/VLF magnetospheric amplification induced by the HAARP facility, *J. Geophys. Res.*, *116*, A04208, doi:10.1029/2010JA016261.

Graf, K. L., N. G. Lehtinen, M. Spasojevic, M. B. Cohen, R. A. Marshall, and U. S. Inan (2013), Analysis of experimentally validated trans-ionospheric attenuation estimates of VLF signals, *J. Geophys. Res. Space Physics*, *118*, 2708–2720, doi:10.1002/jgra.50228.

Harriman, S. K., E. W. Paschal, and U. S. Inan (2010), Magnetic sensor design for femtotesla low-frequency signals, *IEEE Trans. Geosci. Remote Sens.*, *48*, 396–402, doi:10.1109/TGRS.2009.2027694.

Helliwell, R. A. (1970), The upper atmosphere as seen from Antarctica, *Bull. Atom. Sci.*, *26*(10), 55–61.

Helliwell, R. A. (1979), Siple station experiments on wave-particle interactions in the magnetosphere, in *Wave Instabilities in Space Plasmas; Proceedings of the Symposium*, edited by P. J. Palmadesso and K. Papadopoulos, pp. 191–203, D. Reidel Publishing Co., Dordrecht, Netherlands.

Helliwell, R. A. (1983), Controlled stimulation of VLF emissions from Siple Station, Antarctica, *Radio Sci.*, *18*, 801–814, doi:10.1029/RS018i006p00801.

Helliwell, R. A. (1988a), VLF wave stimulation experiments in the magnetosphere from Siple Station, Antarctica, *Rev. Geophys.*, *26*, 551–578, doi:10.1029/RG026i003p00551.

Helliwell, R. A. (1988b), VLF wave-injection experiments from Siple Station, Antarctica, *Adv. Space Res.*, *8*, 279–289, doi:10.1016/0273-1177(88)90373-0.

Helliwell, R. A., and J. P. Katsufrakis (1974), VLF wave injection into the magnetosphere from Siple Station, Antarctica, *J. Geophys. Res.*, *79*(16), 2511–2518, doi:10.1029/JA079i016p02511.

Helliwell, R. A., J. P. Katsufrakis, M. L. Trimpi, and N. M. Brice (1964), Artificially stimulated very low frequency radiation from the ionosphere, *J. Geophys. Res.*, *69*, 2391–2394, doi:10.1029/JZ069i011p02391.

Helliwell, R. A., J. P. Katsufrakis, and M. L. Trimpi (1973), Whistler-induced amplitude perturbation in VLF propagation, *J. Geophys. Res.*, *78*, 4679–4688, doi:10.1029/JA078i022p04679.

Helliwell, R. A., D. L. Carpenter, and T. R. Miller (1980), Power threshold for growth of coherent VLF signals in the magnetosphere, *J. Geophys. Res.*, *85*, 3360–3366, doi:10.1029/JA085iA07p03360.

Hikishima, M., and Y. Omura (2012), Particle simulations of whistler-mode rising-tone emissions triggered by waves with different amplitudes, *J. Geophys. Res.*, *117*, A04226, doi:10.1029/2011JA017428.

Jin, G., M. Spasojevic, M. B. Cohen, U. S. Inan, and N. G. Lehtinen (2011), The relationship between geophysical conditions and ELF amplitude in modulated heating experiments at HAARP: Modeling and experimental results, *J. Geophys. Res.*, *116*, A07310, doi:10.1029/2011JA016664.

Nunn, D., and Y. Omura (2012), A computational and theoretical analysis of falling frequency VLF emissions, *J. Geophys. Res.*, *117*, A08228, doi:10.1029/2012JA017557.

Omura, Y., and D. Nunn (2011), Triggering process of whistler mode chorus emissions in the magnetosphere, *J. Geophys. Res.*, *116*, A05205, doi:10.1029/2010JA016280.

Omura, Y., D. Nunn, H. Matsumoto, and M. J. Rycroft (1991), A review of observational, theoretical and numerical studies of VLF triggered emissions, *J. Atmos. Terr. Phys.*, *53*(5), 351–368, doi:10.1016/0021-9169(91)90031-2.

Omura, Y., Y. Katoh, and D. Summers (2008), Theory and simulation of the generation of whistler-mode chorus, *J. Geophys. Res.*, *113*, A04223, doi:10.1029/2007JA012622.

Otsu, N. (1979), A threshold selection method from gray-level histograms, *IEEE Trans. Syst., Man Cybernet.*, *9*(1), 62–66, doi:10.1109/TSMC.1979.4310076.

Paschal, E. W. (1988), Phase measurements of very low frequency signals from the magnetosphere, PhD dissertation, Stanford University, Stanford, Calif.

Paschal, E. W., and R. A. Helliwell (1984), Phase measurements of whistler mode signals from the Siple VLF transmitter, *J. Geophys. Res.*, *89*, 1667–1674, doi:10.1029/JA089iA03p01667.

Platino, M., U. S. Inan, T. F. Bell, M. Parrot, and E. J. Kennedy (2006), DEMETER observations of ELF waves injected with the HAARP HF transmitter, *Geophys. Res. Lett.*, *33*, L16101, doi:10.1029/2006GL026462.

Raghuram, R., R. L. Smith, and T. F. Bell (1974), VLF Antarctic antenna: Impedance and efficiency, *IEEE Trans. Antennas. Propag.*, *22*, 334–338, doi:10.1109/TAP.1974.1140777.

Sonwalkar, V. S., D. L. Carpenter, R. A. Helliwell, M. Walt, U. S. Inan, D. L. Caudle, and M. Ikeda (1997), Properties of the magnetospheric hot plasma distribution deduced from whistler mode wave injection at 2400 Hz: Ground-based detection of azimuthal structure in magnetospheric hot plasmas, *J. Geophys. Res.*, *102*, 14,363–14,380, doi:10.1029/96JA03047.

Vomvoridis, J. L., and J. Denavit (1979), Test particle correlation by a whistler wave in a nonuniform magnetic field, *Phys. Fluids*, *22*(2), 367–377, doi:10.1063/1.862589.

Watt, A. D. (1967), International series of monographs on electromagnetic waves, in *VLF Radio Engineering*, Pergamon Press, New York.